Radial inversion of 2D potential field data

Valeria C. F. Barbosa(*), LNCC, and João B. C. Silva, UFPA

Abstract

We propose a new 2D method for inverting potential field data with model constraints designed by the interpreter. Our method uses an interpretation model consisting of a source with polygonal cross section whose vertices are described by polar coordinates with an origin inside the source. With this coordinate system, constraints in an inversion are easier to develop and apply. Our inversion method assumes a known physical property contrast for the source and estimates the radii associated with the polygon vertices for a fixed number of equally spaced angles from 0° to 360°. A wide variety of constraints may be used to stabilize the solutions by introducing information about the source shape. The method recovers stable solutions whose shapes range from almost circular or pear-shaped to elongated in one or more directions.

Introduction

We introduce a new potential field inversion method which employs an interpretation model consisting of a 2D homogeneous source with polygonal cross section whose number *M* of vertices and density contrast, together with the coordinates of a point inside the source are specified by the interpreter. The vertices are described in polar coordinates (r_k, θ_k) and the parameters to be estimated are the radii r_k for fixed values of θ_k given by $2\pi(k\text{-}1)/M$. The advantage of the proposed method is that all current stabilizing constraints such as absolute and relative proximity, minimum moment of inertia, and convexity (Silva et al., 2000 and 2001) may be used to incorporate relevant geological information about the source geometry.

Radial method

In this section we present a non-mathematical overview of the method and the applicable constraints. The mathematical and algorithmic details are given in the Appendix.

Consider a homogeneous 2D source with arbitrary cross section S (Figure 1). We approximate the surface *S* by a simple polygon *P* with M sides. Instead of describing *P* by the Cartesian coordinates (x_k, z_k) of its vertices, we describe it by polar coordinates (r_k, θ_k) referred to an arbitrary origin *O* at $(x_o, z_o) \in S$ with the positive *x*-axis being the reference direction for the angle θ, considered positive in the clockwise sense. The number M of sides is established by the interpreter on the basis of his conception about the complexity of true source S. After establishing the value of M, the angles θ_k are given by $2\pi(k\text{-}1)/M,\ k = 1,2,\cdots,M$.

The forward problem consists in establishing the origin *O* and assigning values to the variable M, to $r_k,\ k = 1,2,\cdots,M$, to the density or susceptibility contrast, and, in the case of a magnetic source, to the inclination and azimuth of the magnetization and geomagnetic field vectors, and obtaining the gravity or magnetic anomaly via Talwani et al.'s (1959) and (1965) methods. The inverse problem consists in assigning values to M, to the coordinates of the origin *O*, to the density or susceptibility contrast, and (for a magnetic source) to the inclination and azimuth of the magnetization and geomagnetic field vectors, and estimating the values of $r_k,\ k = 1,2,\cdots,M$ from the observed gravity or magnetic anomaly.

The solution of the unconstrained inverse gravity problem is unique if the density is known and the source belongs to the class of stellar bodies (Novikov, 1938). However, the solution is unstable and stabilizing constraints must be introduced if a geologically meaningful solution is to be obtained. Because all parameters represent the same physical entity (distances between the center O and the vertices), Tikhonov's regularization method, among others, can be used to introduce any of the currently available constraints (Silva et al., 2000 and 2001) as discussed in next section.

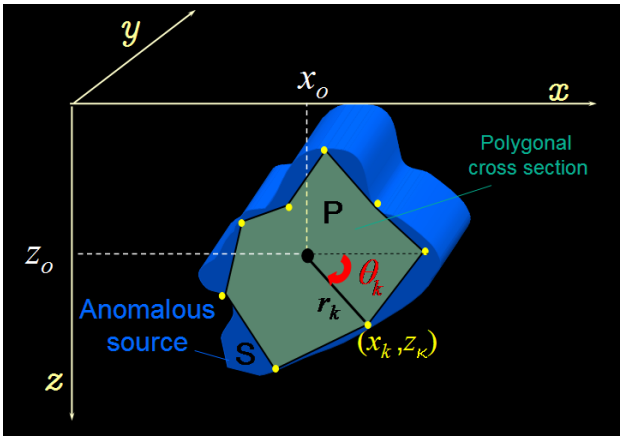

Figure 1- Anomalous source *S* and interpretation model consisting of a polygon *P* whose *k*th vertex is defined by polar coordinates r_k and θ_k.

Even though the assumptions required by the proposed interpretation model are mathematically restrictive, they do not prevent the practical applicability of the method. The premise of a homogeneous source may be (and has been, e.g., Guilllen and Menichetti, 1984) successfully used in important interpretation problems involving anomalous igneous bodies and structures such as batholiths, sills, and laccolithic domes. The physical property contrast required by the method is a geological a priori information which is usually more dependable than the source geometry. The coordinates of the center of

mass (or dipole moment of the source) may be estimated in a stable and reliable way for the class of sources that can be expanded into moments up to second order.

Possible constraints

The absolute and relative proximity constraints (Silva et al., 2001a) and the constraint describing the concentration of anomalous physical property along preferred directions discussed in this section are incorporated by minimizing of the general expression: $\tau = \Psi + \Sigma \mu_j \Phi_j$, $j = 1,2,\cdots,L$, where Ψ is a measure of the data misfit, Φ_j is the functional incorporating the *j*th constraint, and μ_j is a non negative scalar associated with the particular constraint. The inequality and convexity constraints are incorporated in an algorithmic way described below.

Homogeneity and compactness constraints

These constraints are implicitly introduced by the interpretation model itself. They are strong enough to make the inverse problem solution unique and more stable (as will be shown in the next section) as compared with solutions obtained with the currently used interpretation model consisting of a grid of cells.

Inequality constraint

This constraint is introduced by transforming the user-defined constrained parameters into unconstrained parameters, computing estimates for them, and returning to the original constrained parameters. It is used mainly to prevent physical absurdities such as negative radii and negative depths to the top.

Absolute proximity constraint on either all or a few parameters

This constraint requires that $r_{k,}$ be close to pre-specified values $r_{k,}^{o}$, so the functional Φ is given by $\sum_{k=1}^{I} (r_k - r_k^o)^2$, where $I \leq M$. Minimizing Φ favors solutions with a specified geometric feature. In particular, if $I = M$ and all $r_{k,}^{o}$ are constant, the incorporated information is that the source shape is approximately isometric. Nonetheless, even constant $r_{k,}^{o}$ may, in some cases, produce reliable interpretations of particular elongated sources. If $I < M$, minimizing Φ forces a few $r_{k,}$ to be close to a priori known numerical values $r_{k,}^{o}$, $k = 1,2,\cdots,I$, which could be presumed from borehole information.

Relative proximity constraint on all parameters

This constraint requires that all parameters be close to each other. It is incorporated by minimizing the functional $\Phi = (r_M - r_1)^2 + \sum_{k=1}^{M-1} (r_{k+1} - r_k)^2$. As in the case of absolute proximity constraint, the incorporated information asserts that the source shape is approximately isometric, even though reliable interpretations of certain elongated sources may be obtained.

Concentration of the anomalous physical property along preferred directions

This information is introduced via minimization of the functional $\Phi = \sum_{k=1}^{M} (r_k - r_k^o)^2 w_k$, which is a slight modification of the functional used to incorporate absolute proximity constraints. Variables w_k are weights. Small weights are assigned to radii $r_{k,}$ associated with angles θ_k that are close to J specified directions β_j, $j = 1,2,...,J$, along which, the source is assumed to extend. This constraint is useful in interpreting complex sources whose preferred orientations are known. The radii associated with angles θ_k, which are far from the preferred directions, are forced to be close to r_k^o.

Convexity

This attribute is incorporated into the polygon by checking whether the radius r_k is greater than or equal to the distance c_k from the origin *O* to the intersection of the direction of r_k with the line segment joining the vertices (r_{k-1}, θ_{k-1}) and (r_{k+1}, θ_{k+1}). If it is, then r_k is not changed; otherwise, it is set to $r_k = c_k$. This constraint is versatile, leading to reliable interpretations not only of isometric bodies, but also of sources elongated into a single direction. It has been introduced by Zhdanov (1973) but using a different mathematical implementation.

Examples with synthetic gravity data

In all tests we introduce inequality constraints (positivity) on the radii and on the depths to the polygon vertices. In addition, all synthetic anomalies are fitted within the simulated operational errors and all solutions are stable. The solution stability is inferred by inverting theoretical anomalies corrupted with different pseudo random noise sequences and verifying if the solutions are close to each other. In all tests where the functional $\tau = \Psi + \Sigma \mu_j \Phi_j$ is minimized, the value of μ_j was selected as the smallest positive value leading to stable solution.

Laccolithic intrusion

Figure 2 shows the Bouguer anomaly (red dots) produced by the simulated laccolithic intrusion shown in Figure 3 in solid red line having a density contrast ρ of 0.4 g/cm^3. The theoretical anomaly was corrupted with zero-mean Gaussian noise with standard deviation of 0.15 mGal. In all tests using this model we set the origin *O* (white dot, Figure 3) at $x_o = 13$ km, $z_o = 1.5$ km, and $\rho = 0.4$ g/cm^3.

Figure 3a shows the inversion result (dashed line) with $M = 8$ and using just positivity constraint on the radii and on the depths to the polygon vertices. Even though the solution is very far from the true source, it is not completely unrealistic because we, at least, obtain a rough location and an approximate outline of the true source. Rather, if the same anomaly were inverted with the interpretation model consisting of a grid of

homogeneous cells and the parameters to be estimated were the cell densities, the result neither locates nor delineates the true source.

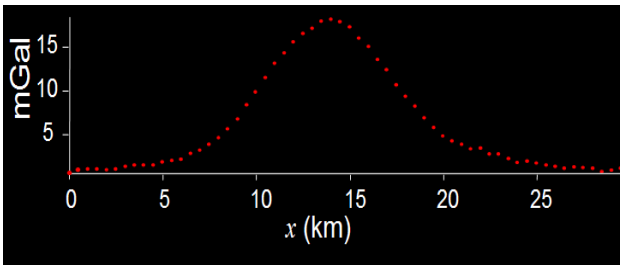

Figure 2 – Noise-corrupted Bouguer anomaly produced by a simulated laccolithic intrusion (solid red line, Figure 3) with $\rho = 0.4$ g/cm^3.

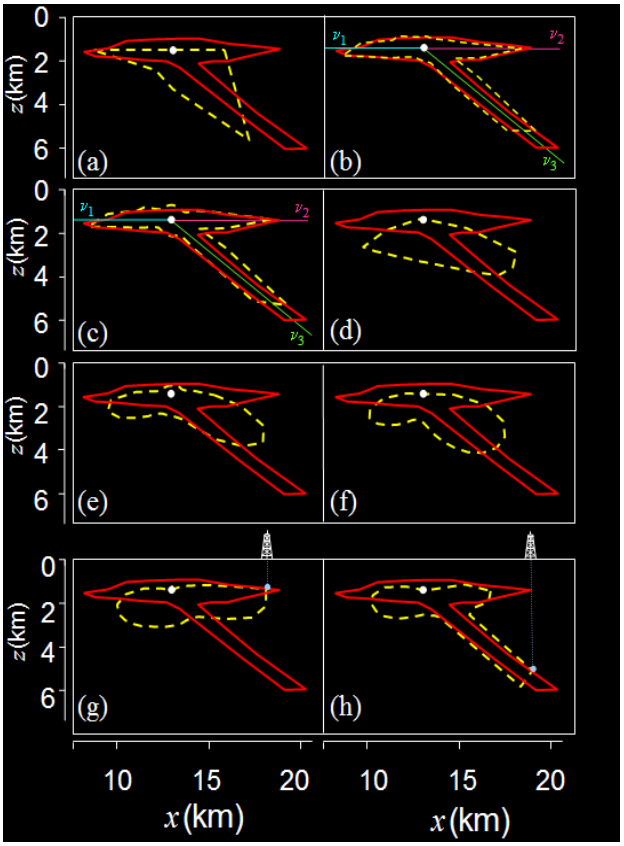

Figure 3 – Inversions of the anomaly shown in Figure 2 using the proposed method. In all tests, positivity constraint is incorporated and the white circle marks the point $O(x_o, z_o)$. (a) Using no additional constraint and $M = 8$; (b) Concentrating the anomalous mass along the preferred directions ν_1, ν_2 and ν_3, with $\mu = 1.2$, $r_k^o = 0.5$ km, and $M = 45$; (c) same as in (b) with $r_k^o = 0.75$; (d) using convexity with $M = 45$; (e) using absolute proximity constraint with $\mu = 1$, $r_k^o = 0.5$ km, and $M = 45$; (f) using relative proximity constraint with $\mu = 0.5$, and $M = 45$; (g) and (h) same as in (f) but constraining the solution upper boundary by information obtained from a single borehole marked by a gray circle with $\mu = 10$ in both cases.

Figure 3b shows the result (dashed line) using as constraint, besides positivity, the concentration of mass along the preferred directions ν_1, ν_2 and ν_3. We used $M = 45$, $\mu = 1.2$, and $r_k^o = 0.5$ km, for all k. The true source geometry is very well estimated. Figure 3c shows the same test as Figure 3b except for the parameter r_k^o now set at 0.75 km, for all k. Note that a convex protrusion shows up around the origin (white dot). If we choose $r_k^o = 0.25$, a concave depression instead of a convex bulge appears around O, indicating that r_k^o should be selected to minimize either bulges or depressions around O. The geologically meaningful results produced by Figures 3b and 3c show that the a priori information that the anomalous mass is concentrated along three directions is an adequate constraint for this type of geologic setting. To illustrate the consequences of using inadequate constraints to interpret this geological setting we will show inversion examples, each one using just one of the following constraints: (1) convexity; (2) absolute proximity; and (3) relative proximity. Figures 3d, 3e, and 3f show, in dashed line, the respective results for the convexity, absolute proximity, and relative proximity constraints on all parameters by setting $M = 45$. For the absolute proximity we used $\mu = 1$ and $r_k^o = 0.5$ km, for all k; for the relative proximity constraint, $\mu = 0.5$ was employed. All three constraints produce poor results indicating that these stabilizing constraints are unsuitable for a laccolithic intrusion interpretation because they bias the inversion toward solutions possessing an attribute not displayed by the true source. To illustrate how an information about the source depth originated from a single borehole can significantly improve the overall shape estimate of the source, we repeated the test shown in Figure 3f with the source boundary constrained to be closest to points $x = 18$ km, $z = 1.5$ km and $x = 19$ km, $z = 5.3$ km with $\mu = 10$ yielding the results shown in dashed line in Figures 3g and 3h, respectively. The latter is just an illustrative test because no borehole is expected to extend to depths of 6 km.

Faulted salt structure

Figure 4 shows the gravity anomaly (red dots) produced by the source shown in Figure 5 in solid red line with $\rho = -0.4$ g/cm^3 and corrupted with zero mean Gaussian noise with standard deviation of 0.25 mGal. This model represents a salt structure and was inspired by a geological interpretation across the Gypsum Valley, eastern Paradox Basin, Colorado. We used $M = 30$, $\rho = -0.4$ g/cm^3, $x_o = 9.5$ km, $z_o = 3$ km, and introduced the relative proximity constraint with $\mu = 0.4$ (dashed line, Figure 5a), the absolute proximity on all parameters with $\mu = 2.0$ and $r_k^o = 1.5$ km, for all k (dashed line, Figure 5b); $\mu = 2.0$, $r_k^o = 0$ km, for all k (dashed line, Figure 5c), and convexity constraint (dashed line, Figure 5d). In Figures 5a and 5b the true source is reasonably delineated because it is roughly isometric and both constraints incorporate this factual property. The test using $r_k^o = 0$ km, for all k (Figure 5c) is the minimum Euclidean norm

estimator, and produces the worst result because all r_k^o closest to zero is not a factual information. The best result consistent with the true source is achieved with the convexity constraint (Figure 5d) which has enhanced the pear-shaped geometry of the source.

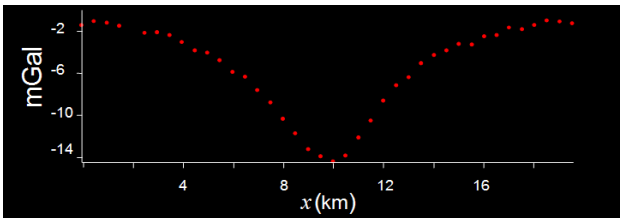

Figure 4 – Noise-corrupted Bouguer anomaly produced by a simulated faulted dome structure intrusion (solid red line, Figure 5) with $\rho = -0.4$ g/cm^3.

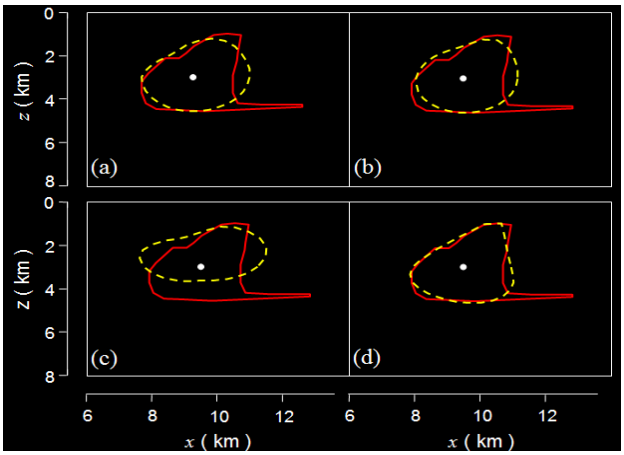

Figure 5 – Inversions of the anomaly shown in Figure 4 using the proposed method. In all tests, positivity constraint is incorporated, $M = 30$ is used, and the white circle marks the point $O\ (x_o, z_o)$. (a) Using relative proximity constraint with $\mu = 0.4$; (b) and (c) using absolute proximity constraint with $\mu = 2$, $r_k^o = 1.5$ km and $\mu = 2$, $r_k^o = 0$ km, respectively, and (d) using convexity constraint.

Lens-shaped pluton

Figure 6 shows the gravity anomaly (dots) produced by the source shown in Figure 7 in solid red line with $\rho = 0.4$ g/cm^3 and corrupted with zero-mean Gaussian noise with standard deviation of 0.15 mGal. We used $M = 32$, $\rho = 0.4$ g/cm^3, $x_o = 10$ km, $z_o = 1.5$ km, and introduced the relative proximity constraint with $\mu = 0.2$ (dashed line, Figure 7a), the absolute proximity on all parameters with $\mu = 1$ and $r_k^o = 0.5$ km, for all k (dashed line, Figure 7b), convexity constraint (dashed line, Figure 7c), and mass concentration along two preferred directions (ν_1 and ν_2 lines in Figure 7d) with $\mu = 1$ and $r_k^o = 0.5$ km, for all k. The relative proximity constraint has a poor performance in delineating the true source, followed by the absolute proximity constraint which reasonably delineates the source. The best performances are achieved by two constraints: (1) convexity (Figure 7c) and (2) concentration of mass along preferred directions (Figure 7d).

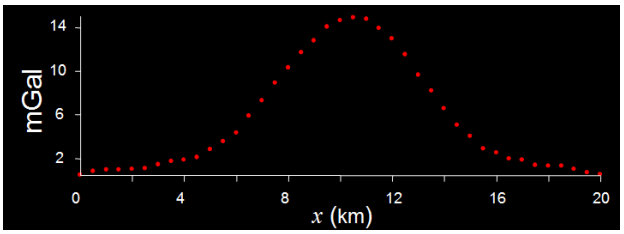

Figure 6 – Noise-corrupted Bouguer anomaly produced by a simulated faulted dome structure intrusion (solid red line, Figure 7) with $\rho = -0.4$ g/cm^3.

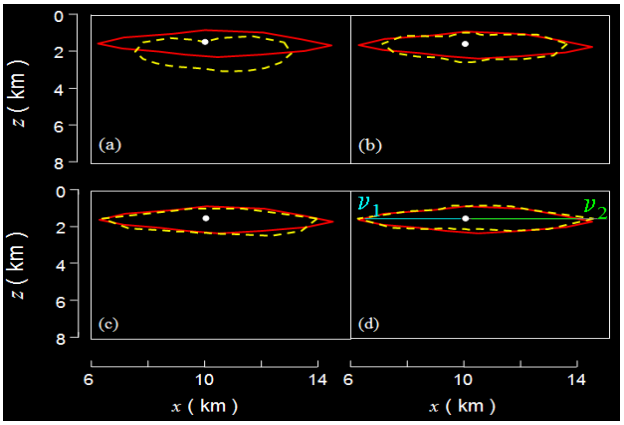

Figure 7 – Inversions of the anomaly shown in Figure 6 using the proposed method. In all tests, positivity constraint is incorporated, $M = 32$ s used, and the white circle marks the point $O\ (x_o, z_o)$. (a) Using relative proximity constraint with $\mu = 0.2$; (b) using absolute proximity constraint with $\mu = 1$, $r_k^o = 0.5$ km; (c) using convexity constraint, and (d) concentrating the anomalous mass along directions ν_1 and ν_2 with $\mu = 1$ and $r_k^o = 0.5$ km.

Real data applications

In all applications in this section we use positivity constraints on the radii and on the depths to the polygon vertices. In all tests, the estimated solutions are stable and fit acceptably the Bouguer anomaly.

Humble dome - Figure 8a shows an east-west profile passing through the center of the Humble Dome Bouguer anomaly (Nettleton, 1976). This anomaly (red dots) has been interpreted by presuming a fixed spherical shape and a known density contrast (Nettleton, 1976). We adapted the proposed method to introduce information about the source extension D_y along the *y*-direction, that, is by assuming that the source is 2½D. We assumed that $\rho = -0.3$ g/cm^3, $M = 31$, D_y =3.5 km and x_o =11.2 km, z_o =4.5 km. The results are shown in Figure 8b using: *i*) relative proximity constraint with $\mu = 0.75$ (solid line) and *ii*) combination of convexity and relative proximity constraints with $\mu = 0.01$ (dashed line). Constraint (*i*) produced a roughly isometric source as imposed a priori

in previous interpretations whereas the combination of constraints (*ii*) produced an alternative interpretation: an elongated source dipping to the east. Both solutions are stable. The fitted anomalies are shown in Figure 8a in solid and dashed lines, respectively.

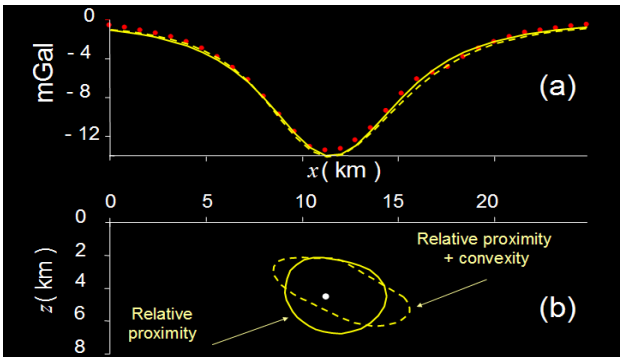

Figure 8 – (a) Bouguer anomaly over Humble dome (red dots). (b) Inversions using positivity constraint, assuming $\rho = -0.3$ g/cm3 and $M = 31$. In solid line is the solution using relative proximity constraint with $\mu = 0.75$, and in dashed line the solution using a combination of convexity, and relative proximity constraints with $\mu = 0.01$. The fitted anomalies (solid and dashed lines) are shown in (a). The white circle marks the point O (x_o, z_o).

Castelsarrasin granitic body - Figure 9a shows the Bouguer anomaly (red dots) produced by the granitic body of Castelsarrasin in the Aquitaine Basin, France (Guillen and Menichetti, 1984). The granitic body was identified by a drill hole that hits its uppermost part at a depth of 500 m (Guillen and Menichetti, 1984). Density contrasts smaller than -0.15 g/cm3 were considered acceptable by Guillen and Menichetti (1984). We applied the proposed method to the above anomaly assuming a 2-D source, $\rho = -0.2$ g/cm^3, $M = 55$, and $x_o =$ 10 km, $z_o =$4 km. The inversion result using convexity constraint (solid line, Figure 9b) shows a preferred orientation which coincides with previous interpretations using explicit a priori information about preferred directions of mass concentration (Guillen and Menichetti, 1984). From the inversion result using just convexity and positivity constraints (solid line, Figure 9b), we defined the preferred directions ν_1 and ν_2. A second inversion result (dashed line, Figure 9b) using the combination of concentration of mass along preferred directions ν_1 and ν_2 (with μ=1 and $r_k^o = 1.5$ km for all k) and convexity constraints, shows an estimated source slightly longer and thinner as compared with the interpretation using just convexity and positivity (solid line, Figure 9b). The fitted anomalies are shown in Figure 9a in solid and dashed lines, respectively.

Conclusions

We have presented a new 2D potential field inversion method which uses an interpretation model consisting of a source with a constant and known physical property contrast and polygonal cross section whose vertices are described by polar coordinates assuming a fixed number of equally spaced angles from 0° to 360° and whose radii are the parameters to be estimated. The present method show that a wide variety of constraints may be easily used to incorporate geological a priori information about the source geometry allowing recovering stable solutions consisting of bodies with shapes ranging from almost circular or pear-shaped to elongated in one or more directions.

Acknowledgments

We are grateful to Dr. Ravat and Dr. Yonghe Sun for their careful revision and constructive criticism that greatly improved the original text. J.B.C.S. was supported in this research by PCI-LNCC-MCT. J.B.C.S. and V.C.F.B were supported by fellowships from CNPq. Additional support for the authors was provided by CNPq under contracts No. 504419/2004-8 and No. 505265/2004-4. One of the authors (V.C.F.B.) was also supported by CNPq (contract No. 472229/03-6) and by CNPq/FAPERJ (contract No. E-26/170.733/2004).

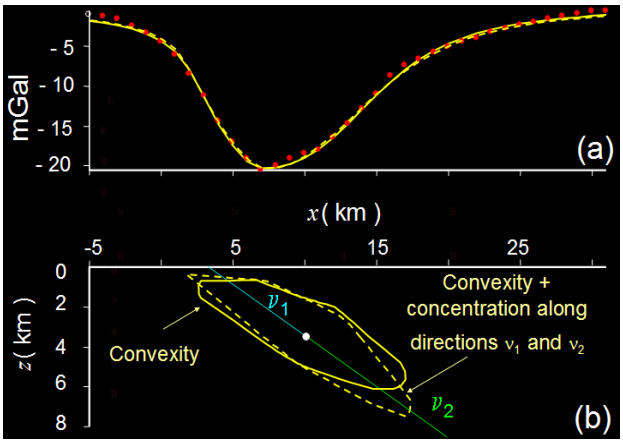

Figure 9 – (a) Bouguer anomaly over the Castelsarrasin granitic intrusion (red dots). (b) Inversions using positivity constraint, $\rho = -0.2$ g/cm3 and $M = 55$. In solid line is the solution using convexity constraint, and in dashed line the solution using a combination of concentration of mass along preferred directions ν1 and ν2 with $\mu = 1$ and $r_k^o = 1.5$ and convexity constraints. The fitted anomalies are shown in (a) in solid and dashed lines, respectively. The white circle marks the point *O* (x_o, z_o).

References

Barbosa, V. C. F., J. B. C Silva, and W. E. Medeiros, 1997, Gravity inversion of basement relief using approximate equality constraints on depths: Geophysics, **62**, 1745-1757

Guillen, A., and Menichetti, V., 1984, Gravity and magnetic inversion with minimization of a specific functional: Geophysics, **49**, 1354-1360.

Nettleton, L. L., 1976, Gravity and magnetics in oil prospecting: McGraw-Hill Book Co.

Novikov, P.S., 1938, Uniqueness of the solution of the inverse problem of potential theory: Bull.Acad. of Sci.USSR,**18** ,165 –168 (in Russian).

Silva, J. B. C, Medeiros, W. E., and Barbosa, V. C. F., 2000, Gravity inversion using convexity constraint: Geophysics, **65**, 102-112.

Silva, J. B. C, Medeiros, W. E., and Barbosa, V. C. F., 2001, Potential field inversion: choosing the appropriate technique to solve a geologic problem: Geophysics, **66**, 511-520.

Talwani, M., Worzel, J.C. and Landisman, M., 1959, Rapid gravity calculations for two-dimensional bodies with application to the Mendocino submarine fracture zone: J. Geophys. Res., **64**, 49-59.

Talwani, M., 1965, Computation with the help of a digital computer of magnetic anomalies caused by bodies of arbitrary shape: Geophysics, **30**, 797-817.

Tikhonov, A. N. and Arsenin, V. Y., 1977, Solutions of ill-posed problems: V. H. Winston & Sons.

Zhdanov, M. S., 1973, Determination of the boundary of the convex body from the gravity potential: Applied Geophysics, **72**, 142-153 (in Russian).

Appendix A- Mathematical Details

Consider a 2D source with a polygonal cross section defined by the radii $r_{k,}$, and angles $\theta_k = 2\pi(k-1)/M$, $k = 1,\cdots,M$ about the origin *O* at (x_o, z_o) (Figure 1). The gravity and magnetic anomaly $f(\mathbf{r})$ produced by such a source may be computed respectively, by Talwani et al.'s (1959) and Talwani`s (1965) methods, where $\mathbf{r}$ is the M-dimensional vector containing the radii r_k. The unconstrained inverse problem consists in estimating $\boldsymbol{r}$ from a set of N observations $\boldsymbol{y}$ via minimization of

$$\Psi(\mathbf{r}) = \left\| \mathbf{y} - f(\mathbf{r}) \right\|^2 , \qquad \text{(A-1)}$$

where $\|\cdot\|$ is the Euclidean norm. To introduce the relative proximity, absolute proximity, and concentration of physical property along preferred directions, we define the stabilizing functionals

$$\Phi_1(\mathbf{r}) = \left\| \mathbf{B}\mathbf{r} \right\|^2 \qquad \text{(A-2)}$$

and

$$\Phi_2(\mathbf{r}) = \left\| \mathbf{W}(\mathbf{r} - \mathbf{r}^{\mathbf{o}}) \right\|^2 , \qquad \text{(A-3)}$$

where $\boldsymbol{B}$ is an $M \times M$ first difference discrete matrix operator (Barbosa et al., 1997), $\mathbf{r}^{\mathbf{o}}$ is a reference parameter vector, and $\boldsymbol{W}$ is a diagonal weighting matrix. To incorporate relative proximity, we minimize Φ_1. To incorporate absolute proximity and concentration of physical property along preferred directions we minimize Φ_2 in the following way. To incorporate absolute proximity constraint, we set $\boldsymbol{W}$ to the identity matrix. To impose concentration of physical property along referred directions β_j, $j = 1,\ldots,J$, we define the kth diagonal element of $\boldsymbol{W}$ as $w_{kk} = \min_j \left\{ \left| \sin[0.5(\beta_j - \theta_k)] \right| + \varepsilon^2 \right\}$, where ε is a small positive number related to the assumed ratio p between the smallest and largest dimensions of the source. Because the maximum weight is one, ε should be close to p.

To incorporate borehole information about the source depth to the top, we proceed in the following way. Let the depth to the source top be known at points $Q_i(r_i, \theta_i)$, $i = 1,\ldots, I$. We determine the index $k(i)$ such that $\theta_{k(i)} < \theta_I < \theta_{k(i)+1}$, where $\theta_{k(i)}$ and $\theta_{k(i)+1}$ are the angles defining the source top ($\pi < \theta_{k(i)} < 2\pi$ and $\pi < \theta_{k(i)+1} < 2\pi$) and associated with the kth polygon vertex which are closest to θ_i. Next, we find the projections $b_{i,k(i)}$ and $b_{i,k(i)+1}$ of Q_i on the straight lines coinciding with the directions of $r_{k(i)}$ and $r_{k(i)+1}$. The lengths of radii $r_{k(i)}$ and $r_{k(i)+1}$ are then forced to be closest to projections $b_{i,k(i)}$ and $b_{i,k(i)+1}$ by minimizing the functional

$$\Phi_3 = \sum_{i=1}^{I} (r_{k(i)} - b_{i,k(i)})^2 + (r_{k(i)+1} - b_{i,k(i)+1})^2 . \qquad \text{(A-4)}$$

All the above constraints are introduced into the unconstrained problem of minimizing functional (A-1) by minimizing

$$\tau = \Psi(\mathbf{r}) + \mu_1 \Phi_1(\mathbf{r}) + \mu_2 \Phi_2(\mathbf{r}) + \mu_3 \Phi_3(\mathbf{r}), \qquad \text{(A-5)}$$

where μ_1, μ_2 and μ_3 are non negative scalars. The inequality and convexity constraints are introduced algorithmically and will be described later. Functional (A-5) is nonlinear in $\mathbf{r}$ and is minimized via Newton's method. The inequality constraints used in the present method prevent the radii from becoming smaller than zero and greater than geological or physical limits defining the vector $\mathbf{r}_{\max}$. These constraints are expressed as

$$\mathbf{0} < \mathbf{r} < \mathbf{r}_{\max} , \qquad \text{(A-6)}$$

where $\mathbf{0}$ is the null vector and the inequality sign is applied element by element. The kth element of vector $\mathbf{r}_{\max}$ is given either by

$$r_{\max_k} = q, \qquad 0 \le \theta_k \le \pi \qquad \text{(A-7)}$$

where q is a very large positive number, or by

$$r_{\max_k} = \frac{z_o}{\text{abs}[\sin(\theta_k)]}, \qquad \pi < \theta_k < 2\pi. \qquad \text{(A-8)}$$

Condition (A-7) establishes a limit for the source base whereas condition (A-8) prevents the *z*-coordinates of the polygon vertices from becoming negative. The inequality constraints (A-6) are incorporated by *i*) transforming the original parameter vector $\mathbf{r} \equiv \{r_k\}, \in (0, r_{\max_k})$ $k = 1,\ldots, M$ into the unconstrained parameter vector $\mathbf{r}^* \equiv \{r_k^*\}, \in (-\infty, +\infty)$ $k = 1,\ldots, M$ by the homeomorphic transformation.

The convexity constraint is introduced algorithmically by checking at each iteration the inequality $r_k \ge c_k$, $k = 1,\cdots,M$, where c_k is the distance from the center O to the intersection of the direction of r_k with the line segment joining the vertices (r_{k-1}, θ_{k-1}) and (r_{k+1}, θ_{k+1}). If the inequality holds, the estimate of r_k at the current iteration is unchanged; otherwise, it is set to c_k.